Journal of the American Heart Association

ORIGINAL RESEARCH

Aging-Associated ALKBH5-m^{6}A Modification Exacerbates Doxorubicin-Induced Cardiomyocyte Apoptosis Via AT-Rich Interaction Domain 2

Runtai Chen, MD, PhD; Guogang Zhang, MD, PhD; Kun Sun, MD, PhD; Alex F. Chen, MD, PhD

BACKGROUND: Chemotherapy-induced cardiovascular disease is a growing concern in the elderly population who have survived cancer, yet the underlying mechanism remains poorly understood. We investigated the role of ALKBH5 (AlkB homolog 5), a primary N^6-methyladenosine (m^{6}A) demethylase, and its involvement in m^{6}A methylation-mediated regulation of targets in aging-associated doxorubicin-induced cardiotoxicity.

METHODS AND RESULTS: To validate the relationship between doxorubicin-induced cardiotoxicity and aging, we established young and old male mouse models. ALKBH5 expression was modulated through adeno-associated virus 9 (in vivo), *Lentivirus*, and siRNAs (in vitro) to examine its impact on cardiomyocyte m^{6}A modification, doxorubicin-induced cardiac dysfunction, and remodeling. We performed mRNA sequencing, methylated RNA immunoprecipitation sequencing, and molecular assays to unravel the mechanism of ALKBH5-m^{6}A modification in doxorubicin-induced cardiotoxicity. Our data revealed an age-dependent increase in doxorubicin-induced cardiac dysfunction, remodeling, and injury. ALKBH5 expression was elevated in aging mouse hearts, leading to reduced global m^{6}A modification levels. Through mRNA sequencing and methylated RNA immunoprecipitation sequencing analyses, we identified ARID2 (AT-rich interaction domain 2) as the downstream effector of ALKBH5-m^{6}A modulation in cardiomyocytes. Further investigations revealed that ARID2 modulates DNA damage response and enhances doxorubicin-induced cardiomyocyte apoptosis.

CONCLUSIONS: Our findings provide insights into the role of ALKBH5-m^{6}A modification in modulating doxorubicin-induced cardiac dysfunction, remodeling, and cardiomyocyte apoptosis in male mice. These results highlight the potential of ALKBH5-targeted treatments for elderly patients with cancer in clinical settings.

Key Words: aging ■ ALKBH5 ■ cardiotoxicity ■ doxorubicin ■ m^{6}A

Over the past few decades, the development of chemotherapy and chemotherapy-based combination therapies has revolutionized cancer treatment, leading to a significant reduction in cancer-related mortality. However, despite these remarkable advancements, the risk of side effects associated with chemotherapy on normal cells and specific organs remains a major concern, imposing limitations on the applicable dosages. One such adverse effect is chemotherapy-induced cardiotoxicity, which is particularly relevant in the context of doxorubicin treatment.

Correspondence to: Alex F. Chen, MD, PhD and Kun Sun, MD, PhD, Institute for Developmental and Regenerative Cardiovascular Medicine, Xinhua Hospital, Shanghai Jiao Tong University School of Medicine, No.1665 Kongjiang Road, Shanghai 200092, China. Email: chenfengyuan@xinhuamed.com.cn; sunkun@xinhuamed.com.cn

This article was sent to Rebecca D. Levit, MD, Associate Editor, for review by expert referees, editorial decision, and final disposition.

Supplemental Material is available at https://www.ahajournals.org/doi/suppl/10.1161/JAHA.123.031353

For Sources of Funding and Disclosures, see page 17.

JAHA is available at: www.ahajournals.org/journal/jaha

RESEARCH PERSPECTIVE

What Is New?

- The aging process contributes to ALKBH5 (AlkB homolog 5)-mediated m^{6}A modification in heart, consequently influencing the DNA damage repair via AT-rich interaction domain 2.
- ALKBH5-mediated m^{6}A regulation shows promise as a target for preventing or treating chemotherapy-induced cardiotoxicity during aging.

What Question Should Be Addressed Next?

- Further research will primarily concentrate on investigating the sex difference in aging-associated ALKBH5-m^{6}A modification in heart, establishing a doxorubicin-induced cardiotoxicity model using tumor (ALKBH5 knockout or overexpression cancer cells)-bearing nude mice and exploring more detailed mechanism underlying the basal posttranslational modification difference between cancer and cardiomyocytes.

Nonstandard Abbreviations and Acronyms

AAV	adeno-associated virus
ALKBH5	AlkB homolog 5
AngII	angiotensin II
ARID2	AT-rich interaction domain 2
BRD7	bromodomain containing 7
cTnT	cardiac-specific troponin T
DIC	doxorubicin-induced cardiotoxicity
FTO	fat mass and obesity-associated gene
m^{6}A	N^6-methyladenosine
MeRIP	M^{6}A-RNA immunoprecipitation
METTL14	methyltransferase 14
METTL3	methyltransferase 3
PBRM1	polybromo 1
siRNA	small interfering RNA
WT	wild-type

Doxorubicin, a widely used chemotherapeutic agent, has demonstrated efficacy in combating cancer. However, its clinical use is hampered by its potential to induce myocardial dysfunction and heart failure, commonly referred to as cardiotoxicity. This detrimental effect of doxorubicin significantly contributes to premature morbidity and mortality among survivors of cancer, particularly in the elderly population.[1]

The understanding of doxorubicin-induced cardiotoxicity (DIC) is still insufficient for effective prevention. The current mechanistic understanding of DIC primarily revolves around the increased formation of reactive oxygen species and targeting of topoisomerase 2β in cardiomyocytes, resulting in cardiomyocyte death.[2] However, it has been observed that the risk of doxorubicin-induced cardiotoxicity is not solely dependent on comorbidities and performance status but also increases with advancing age. This age-associated risk suggests the involvement of additional factors and molecular pathways in the development of doxorubicin-induced cardiotoxicity.[3]

In recent years, the field of RNA modifications has emerged as a promising area of research in cardiovascular biology. Among the various types of RNA modifications, N^6-methyladenosine (m^{6}A) modification has gained substantial attention. m^{6}A modification is the most prevalent form of internal posttranscriptional RNA modification and can be dynamically regulated by m^{6}A methyltransferases (such as METTL3 [methyltransferase 3] and METTL14 [methyltransferase 14]) and demethylases (such as *FTO* [fat mass and obesity-associated gene] and ALKBH5 [AlkB homolog 5]).[4] Studies have highlighted the emerging roles of m^{6}A modification in a range of cardiac conditions, including ischemic heart failure,[5] cardiomyocyte proliferation, heart regeneration,[6] heart hypertrophy,[7–9] and cardiac fibrosis[10] and doxorubicin-induced cardiomyocyte damage.[11] Additionally, dysregulation of m^{6}A methylation has been linked to the aging process, further emphasizing its relevance in age-associated diseases.[12,13]

In this study, we demonstrate an age-associated increase in the expression of ALKBH5, a key demethylase involved in m^{6}A modification, in the heart. We further establish that elevated ALKBH5 expression exacerbates doxorubicin-induced cardiac dysfunction. Additionally, through our investigations, we identify AT-rich interaction domain 2 (*ARID2*) as the target gene modulated by ALKBH5, which contributes to doxorubicin-induced cardiomyocyte apoptosis by modulating DNA damage response. Our findings shed light on the potential detailed mechanisms underlying aging-associated DIC and emphasize the clinical significance of ALKBH5-m^{6}A modification in the prevention or mitigation of cardiotoxicity among elderly patients with cancer.

METHODS

The data presented in this study are available from the corresponding author upon reasonable request.

Animal Studies

C57BL/6J male mice were obtained from The Hunan Slac Laboratory Animal Company (Changsha, China)

and The Nanjing Qingzilan Technology Co., Ltd. (Nanjing, China), respectively. Considering mice have a lifespan of approximately 2.5 to 3 years and are ideally suited for aging studies, male mice at 3 months (young group) or 20 to 24 months (old group) old were used. The 24-month-old mice were used for measurement of m^6A methylation level and its related enzymes, and the 20-month-old mice were used for establishing doxorubicin-induced cardiotoxicity in the context of aging. Before the start of the experiment, all animals underwent thorough health assessments to ensure that only healthy animals were included. Animals showing any signs of illness, infections, or immune compromise were excluded from the study. All animal care protocols and experiments were reviewed and approved by the Animal Care and Use Committees of the Laboratory Animal Research Center at Xiangya Medical School of Central South University. The investigation conforms to the *Guide for the Care and Use of Laboratory Animals* published by the US National Institutes of Health (NIH Publication No. 85–23, revised 1985).

Experimental Design and AAV Vector

Mice were injected with a cumulative dose of 20 mg/kg doxorubicin (doxorubicin) or saline via 4 weekly intraperitoneal injections (5 mg/kg IP, doxorubicin groups). These mice were observed daily and weighed every week. After a 4-week doxorubicin insult, echocardiography detections were performed. Then the mice were euthanized with an overdose of sodium pentobarbital (200 mg/kg IP) for rapid sample collection. Mice hearts and tibia were collected to calculate heart weight/tibia length ratios. Heart samples were processed for subsequent biochemical and histological analyses. The upper half of the heart was fixed in 4% paraformaldehyde for 24 hours, dehydrated, and embedded in paraffin for histological analysis, enabling the preservation of tissue architecture. The lower half of the heart was flash frozen in liquid nitrogen, preserving molecular components for biochemical analysis. This precise tissue processing methodology ensures reliable assessment of both molecular and cellular parameters in cardiac research.

To specifically overexpress ALKBH5 in the myocardium, each 3-month wild-type (WT) mouse received a single intravenous injection (8×10^{11} viral genomes per mouse) of type adeno-associated virus vector 9 (AAV9) containing ALKBH5, eGFP (enhanced green fluorescent protein) and cTnT (cardiac-specific troponin T) promoter (AAV9-ALKBH5) in a 200-μL volume into the tail vein. AAV9-cTnT-GFP served as negative control (AAV9-vector).

To specifically downregulate ALKBH5 in the myocardium, each 20-month WT mouse received a single intravenous injection (1×10^{12} viral genomes per mouse) of AAV9 containing shRNA targeting ALKBH5, eGFP, and cTnT promoter (AAV9-shALKBH5) in a 200-μL volume into the tail vein or negative control via the tail vein. shRNA targeting mouse *ALKBH5* gene was created in the 19 bp sequence ACAAGTACTTCTTCGGCGA in an AAV9 vector. AAV9-cTNT-GFP-RNAi served as negative control (AAV9-shctrl). All AAV9 viruses mentioned were constructed by Shanghai GeneChem Co. Ltd. (Shanghai, China).

Transthoracic Echocardiography

Mice were lightly anesthetized with 1% of isoflurane until the heart rate stabilized at 350 and 450 bpm and kept on a 37 °C heated plate throughout the procedure. In vivo cardiac function was assessed by transthoracic echocardiography using a Vevo 1100 imaging system (VisualSonics, Fujifilm) with a linear probe 40 MHz frequency. Heart rate, end-systolic diameter, end-diastolic diameter, fractional shortening, and ejection fraction were calculated with Vevo Analysis software as described previously.[14] Studies and analyses were performed blinded to the heart condition.

Blood Serum Measurement

Blood samples were obtained from the heart by cardiac puncture, preferably from the ventricle. Blood was collected in the microtube and allowed to clot at 4 °C overnight followed by 15 minutes centrifugation at 2500 rpm. Serum was immediately aliquoted and kept at −80 °C until use. The measurements of mouse creatine kinase MB isoenzyme and cTnT in plasma were performed using an ELISA kit (Huamei, Wuhan, China) according to manufacturer's instructions.

Histological Analysis

Hearts from each group were rapidly excised and washed in cold PBS. A portion of the hearts was cut off and fixed in 4% formalin and embedded in paraffin, and 5 μm-thick heart tissue slices were dewaxed, rehydrated, and subjected to hematoxylin–eosin staining and Masson staining for evaluation of cross-section cardiomyocyte and cardiac fibrosis. Bright-field images of the same samples were captured after the histological staining process. The cross-section cardiomyocyte area and the positive area were evaluated using ImageJ software.

Immunofluorescence

Cells seeded on coverslips were fixed in 3.7% formaldehyde in PBS for 15 minutes at indicated time points. Then cells were washed with PBS and permeabilized for 10 minutes in 0.1% TritonX-100/PBS. After permeabilization, blocking buffer (5% bovine serum albumin in 0.1% Triton/PBS) was added for 1 hour, followed by

incubation with γ-H2AX (phospho-histone H2A.X, rabbit recombinant, Cell Signaling, ref 7631S) overnight at 4 °C. After being washed with PBS, cells were incubated with Alexa 594 antirabbit fluorescent secondary antibodies (Proteintech, 1:200 dilution) in the dark for 2 hours at room temperature. The nuclei were counterstained with 4′,6-diamidino-2-phenylindole (DAPI, Beyotime, C1002). Images were acquired using Zeiss LSM800 confocal microscope and foci of phospho-H2AX were quantified using ImageJ software.

For cardiac troponin I staining, sections were blocked with PBS containing 10% fetal bovine serum for 1 hour and then stained overnight at 4 °C in 0.5% BSA with 10 μg/mL of anticardiac troponin I antibody (#66376-1-Ig, Proteintech, 1:200 dilution). Secondary staining was performed with 10 μg/mL of goat anti-mouse IgG (H+L) (#SA00007-1, Proteintech) for 30 minutes and then subsequently stained with DAPI. Images were collected on a Carl Zeiss epifluorescence-equipped inverted microscope.

Terminal Deoxynucleotidyl Transferase dUTP Nick End Labeling Assay

TUNEL (terminal deoxynucleotidyl transferase dUTP nick end labeling) staining was used to evaluate cardiac apoptosis according to the manufacturer's instruction (in situ cell death detection kit, TMR red, Sigma-Aldrich). Apoptosis was indicated as the ratio of TUNEL-positive nuclei/DAPI-stained nuclei in 3 images per heart.

RNA Isolation, cDNA Preparation, and Reverse Transcriptase–Polymerase Chain Reaction

Total RNA isolation from mice hearts was performed with Trizol reagent (Invitrogen) according to the manufacturer's protocol. RNA concentration was immediately quantified using nanodrop 2000 (Fisher Scientific), and RNA samples were stored as aliquots at −80 °C. For cDNA synthesis, 1 μg total RNA was transcribed with PrimeScript™ RT Master Mix (Takara, RR036A) according to the manufacturer's instructions. For gene expression analysis, cDNA was amplified by quantitative reverse transcriptase–polymerase chain reaction (RT-PCR) with SYBR Green PCR Master Mix (Bio-Rad) and gene-specific primers. Primers were designed using PrimerBank and are listed in Table S1. All samples were run in triplicate. Relative expression was determined using the ΔΔCT method.

Western Blotting

Heart tissues were homogenized by high-speed vibrating ball miller (Tiss-24, Jingxin, Shanghai) in RIPA buffer (Beyotime, China) supplemented with protease and phosphatase inhibitors (Beyotime, China) on the ice before sonication. Protein concentrations were quantified using a BCA kit (KGP902, keygentec, Jiangsu, China) according to the manufacturer's protocol. Total protein lysates (30 μg) were separated on sodium dodecyl sulfate-polyacrylamide gel electrophoresis and transferred to polyvinylidene fluoride membranes (100 V for 100 minutes at 4 °C).

The membrane was blocked with 5% milk in Tris-buffer-saline supplemented with 1% Tween-20 and incubated with primary antibodies for 1 hour at room temperature. Antibodies were directed against METTL3 (rabbit polyclonal, Cell Signaling, ref 96391S), METTL14 (rabbit polyclonal, Cell Signaling, ref 51104S), FTO (rabbit recombinant, Abcam, ab126605), ALKBH5 (rabbit recombinant, Abcam, ab195377), AARID2 (rabbit polyclonal, Proteintech, 23406-1-AP), PBRM1 (polybromo 1, rabbit polyclonal, Proteintech, 12563-1-AP), BRD7 (bromodomain containing 7, rabbit polyclonal, Proteintech, 51009-2-AP), γ-H2AX (rabbit recombinant, Cell Signaling, ref 7631S), and GAPDH (rabbit polyclonal, Proteintech, 10494-1-AP). The secondary antibody was incubated for 1 hour at room temperature. Subsequently, the blot was extensively washed with PBS and exposed to enhanced chemiluminescence detection reagents (Adcansta, USA) according to the manufacturer's instructions. The immune complex is visualized by ChemiDocTM MP Imaging System (Bio-Rad, CA). Quantification and analysis were performed using the Image Lab software (Version 5.1, Bio-Rad).

Cell Culture

AC16 adult human ventricular cardiomyocytes were purchased from Sigma-Aldrich Inc. (SCC109, Sigma, Santa Clara, CA) and cultured in DMEM-F12 medium with 10% fetal bovine serum (Gibco) and 1% penicillin-streptomycin (Gibco) at 37 °C in a humidified incubator containing 5% CO_2. The human breast cancer cell line MCF-7 was obtained from American Type Culture Collection with authentication. These cell lines were cultured inDMEM (Corning, NY) with 10% fetal bovine serum and antibiotics. Cells were grown in a 5% CO_2 cell culture incubator at 37 °C.

RNA Methylation Quantification

The quantification of the m^6A RNA methylation levels in heart mRNA of young and old mice was detected using an EpiQuik™ m^6A RNA methylation quantification kit (EpiGentek) as described by the manufacturer. In brief, messenger RNA was isolated from cells and bound to a strip well for 90 minutes. Each well was washed and the captured antibody, detection antibody, and enhancer solution were added. The color-developing solution was then added, and the absorbance at 450 nm was measured.

Finally, to determine the relative m^{6}A RNA methylation status, the calculation for the percentage of m^{6}A in RNA was carried out using the following formula:

$$\text{m6A}\% = \frac{(\text{Sample OD} - \text{NC OD}) \div S}{(\text{PC OD} - \text{NC OD}) \div P} \times 100\%.$$

NC (Negative Control, 100 μg/mL), PC (Positive Control, m^{6}A 2 μg/mL). *S* is the amount of input sample RNA in ng. *P* is the amount of input positive control (PC) in ng.

m^{6}A Dot Blot Assay

RNA isolation was isolated from fresh heart tissue as previously described. Notably, for dot blot assay, the concentration of purified mRNA should be at least 20 μg, and a dilution of mRNA to 100 ng/μL should be made using RNase-free water. The diluted mRNA was denatured for 3 minutes at 95 °C and was immediately chilled on ice. The mRNA sample (2 μL) was applied to an N+ nylon membrane (Magna Nylon, Osmonics Inc., pore size 0.45 μm) and ultraviolet-crosslinked using a crosslinking device (CL-1000, UVP). After blocking in blocking buffer (PBS with 0.1% Tween 20 and 5% nonfat milk) for 1 hour at room temperature, the membranes were incubated overnight at 4 °C using an anti-m^{6}A antibody (1:1000 dilution in blocking buffer; ABE572, Millipore Sigma). Then, the membranes were incubated with secondary antibodies and exposed using a ChemiDocTM MP Imaging System (Bio-Rad, CA). Notably, all membrane incubation and washing should be done with gentle shaking. The same amount of RNA was spotted on the membrane, stained with 0.02% methylene blue in 0.3 mol/L sodium acetate (pH5.2) for 2 hour, and washed with ribonuclease-free water for 5 hours.

Induction of Cell Senescence

Briefly, AC16 cardiomyocytes were exposed to hydrogen peroxide (H_2O_2) at concentrations of 25, 50, 100, or 200 μmol/L or angiotensin II (AngII) at concentrations of 50, 100, 200, or 400 μmol/L, for 2 hours in a 5% CO_2 cell culture incubator at 37 °C. After the treatment, H_2O_2 or AngII-containing medium is carefully removed and replaced with fresh growth medium. The cells were then further incubated in the fresh growth medium for an additional 72 hours at 37 °C. For subsequent in vitro experiments, unless stated otherwise, a concentration of 100 μmol/L H_2O_2 and 200 μmol/L AngII was employed.

Senescence-Associated β-galactosidase Staining Assay

SA-β-gal (senescence-associated β-galactosidase) staining of AC16 cells was performed using an SA-β-gal staining kit (Beyotime Biotechnology, China; Cat#C0602) according to the manufacturer's protocol. In brief, cells were fixed in 4% paraformaldehyde for 10 minutes. After washing twice with PBS, samples were incubated in SA-β-gal solution at 37 °C overnight. Ice-cold PBS was then used to stop the enzymatic reaction. In blinded analyses, for each sample, 3 images were taken from random fields using a microscope. The ratio of positive cells was determined by counting the blue cells and dividing by the total number of observed cells.

Luciferase Reporter Gene Assay

The 3′UTR of ARID2 was cloned into pmiGLO vector (Tsingke, China). Three putative m^{6}A recognition site bases (A) were mutated into bases (T) in 3′UTR using a Site-Directed Mutagenesis Kit (Thermo) according to the instruction. The WT and Mut plasmids were transfected in AC16 cells (transfection is described in detail in the next part), and then the Dual-Luciferase Reporter Gene Assay Kit (Beyotime Biotechnology, China; Cat#RG027) was used for detecting the luciferase activity according to the instructions. All samples were measured by the Victor multilabel plate reader (PerkinElmer).

Cell Transfection

Lipofectamine 3000 (#2067450, Invitrogen) was used to deliver small interfering RNAs (siRNAs, including Control, ALKBH5, YTHDC1–2 [YTH domain-containing family protein], YTHDF1–3 [YTH N6-methyladenosine RNA binding family protein], ARID2) and plasmids (including ARID2 WT and 3 mutants, empty vector, and ARID2) into AC16 cells. The transient transfection methods were carried out according to the manufacturer's instructions. These transfected cells were analyzed after 48 hours. ARID2 overexpression vectors and empty vectors were constructed by GeneChem (Shanghai, China). GFP-vector lentivirus and GFP-ALKBH5 lentivirus were constructed by GeneChem (Shanghai, China). For ALKBH5 and scramble overexpression, the ALKBH5 complementary DNA sequence was inputted to Shuffle DNA (http://www.bioinformatics.org/sms2/shuffle_dna.html) to generate a scrambled sequence. The ALKBH5 and scramble sequences were then synthesized and cloned into an overexpression vector. AC16 cells were transfected with various plasmids using lentivirus according to the manufacturer's instructions. Stable clonal cell lines were selected with 2 μg/mL puromycin. The sequences of siRNAs and primers are listed in Table S2.

RNA Immunoprecipitation Sequencing

An RNA limmunoprecipitation (RIP) experiment was performed according to the instructions of the Magna

RIP RNA Binding Protein Immunoprecipitation Kit (Millipore, MA). Briefly, the lysate was prepared in a lysis buffer containing a protease inhibitor cocktail and RNase inhibitor. Then, protein A/G magnetic beads were prepared for incubation with 5 μg of purified antibodies per immunoprecipitation with rotation for 30 minutes at room temperature. Further, to precipitate RNA-binding protein-RNA complexes, the mixture was incubated with rotation for 3 hours overnight at 4°C. Finally, RNA was purified using proteinase K buffer and an Agilent 2100 Bioanalyzer (Agilent, CA). A NanoDrop 2000 (Thermo Fisher) was used to analyze the total RNA quality and quantity. Further RNA purification in immunoprecipitation may be pursued by deep sequencing or quantitative RT-PCR. The cDNA libraries were sequenced on the Illumina sequencing platform by Genedenovo Biotechnology Co., Ltd. (Guangzhou, China).

Based on the documented procedure, total RNA was extracted using Trizol reagent (Invitrogen) following the manufacturer's procedure. The total RNA quality and quantity were analyzed of Bioanalyzer 2100 and RNA 6000 Nano LabChip Kit (Agilent) with RIN number >7.0. Approximately >50 μg of total RNA was subjected to isolate Poly(A) mRNA with poly-T oligo attached magnetic beads (Invitrogen). The cleaved RNA fragments were subjected to incubation for 2 hours at 4 °C with an m^{6}A-specific antibody (No. 202003, Synaptic Systems, Germany) in IP buffer (50 mmol/L Tris–HCl, 750 mmol/L NaCl, and 0.5% Igepal CA-630) supplemented with BSA. The mixture was then incubated with protein-A beads and eluted with elution buffer (1×IP buffer and 6.7 mmol/L m^{6}A). Eluted RNA was precipitated by 75% ethanol. Eluted m^{6}A-containing fragments (IP) and untreated input control fragments are converted to the final cDNA library following a strand-specific library preparation by the dUTP method. Then we performed the paired-end 2×150 bp sequencing on an Illumina Novaseq™ 6000 platform at the LC-BIO Biotech Ltd (Hangzhou, China) following the vendor's recommended protocol. For RIP-seq, input mRNAs and IP with 150 to 200 ng RNA of each sample were used to generate the library using the Illumina kit.

M^{6}A-RNA Immunoprecipitation Assay, m^{6}A Sequencing, and mRNA-Sequencing Analysis

Total RNAs were first extracted from stable ALKBH5 overexpression AC16 cells and their corresponding nontarget controls. Chemically fragmented RNA (~100 nt) was incubated with an m^{6}A antibody for immunoprecipitation according to the standard protocol of Magna MeRIP™ m^{6}A Kit (Merck Millipore). The Magna ChIP Protein A/G Magnetic Beads were incubated for 30 minutes at room temperature with m^{6}A-specific antibody in immunoprecipitation buffer. The mixture was then incubated with the M^{6}A-RNA immunoprecipitation (MeRIP) reaction mixture for 2 hours at 4 °C. Finally, RNA was purified using the RNeasy MinElute Cleanup kit (#74204, QIAGEN). Eluted RNA and MeRIPed RNA were then analyzed either through high-throughput sequencing or by quantitative RT-PCR. For high-throughput sequencing, purified RNA fragments from m^{6}A-MeRIP were analyzed by deep sequencing on an Illumina Novaseq™ 6000 platform at the LC-BIO Biotech Ltd (Hangzhou, China) following the vendor's recommended protocol. mRNAs showing significant (P<0.05) and at least 2-fold changes in m^{6}A levels, mRNA levels, and polysome binding are reported in this study. Differential m^{6}A methylation was further verified using quantitative RT-PCR with the primers listed in Table S1 on RNAs immunoprecipitated with anti-m^{6}A antibodies without fragmentation. For mRNA-sequencing analysis, total RNA extraction was performed as described and analyzed at LC-BIO Biotech Ltd (Hangzhou, China). We used the ClueGo plug-in in the Cytoscape software for pathway analysis for genes identified in different experiments.

RNA Stability Assay

AC16 cells were seeded in a 6-well plate and transfected with vector or ALKBH5-overexpressed plasmid for 48 hours. Then, actinomycin D (A9415, Sigma-Aldrich) at 5 μM was added to the cells. After an indicated treatment time (t=0, 1, 2, 4, 6 hours), cells were harvested and total RNA was isolated and analyzed by quantitative RT-PCR analysis. Results were processed with Microsoft Excel and then normalized to the t=0 time point. Fold differences in expression levels were calculated according to the $2^{-\Delta CT}$ method. ΔCt=(average Ct of each time point–average Ct of t=0). Half-life ($t_{1/2}$) of ARID2 mRNA was calculated using GraphPad.

Statistical Analysis

Echocardiographic analyses were performed blind to the treatment group. The first author Runtai Chen was aware of the group allocation at the different stages of the experiment. Data are presented as mean±SEM. Between-group differences were calculated with Student's t test, 1-way ANOVA, or 2-way ANOVA as appropriate. Statistical tests including Dunnett's test, Tukey post hoc test, and Sidak's test were used for each data set. Statistical significance was defined as P<0.05. Each data point represents a separate biological replicate (mouse/experiment). Statistical analyses were undertaken using Prism software (San Diego, CA).

The sample size of the mouse experiments was determined following a power calculation (with a power of 0.8 and alpha of 0.05) by using ejection fraction data from previously published studies.[14,15] Differences in means (13%) and SDs (0.07 and 0.06) were derived from the study by Pan,[14] and differences in means (10%) and SDs (0.06 and 0.046) were obtained from the study by Gupta.[15] An effect size of 2 was calculated using Cohen's *D* method. From the literature, on average, 6 mice per group were used for the establishing doxorubicin-induced cardiotoxicity model and following functional and structural measurements. Animals were randomly assigned to either vehicle or treatment groups using a computer-generated random number generator. We minimized potential confounders by using randomization and counterbalancing for treatment order and measurements. No animals, experimental units, or data points were excluded in the analysis. Generally, we used the Shapiro–Wilk test for the normality test of the data. In addition, the distribution of these variables in our study (heart ejection fraction, serum cardiac injury markers levels, etc) in the population is assumed to be normal.

RESULTS

ALKBH5-m^{6}A RNA Methylation Level Decreased in the Heart During Aging

To determine whether RNA m^{6}A methylation was involved in the aging-associated deterioration effect of doxorubicin-induced cardiotoxicity, a natural aging mouse model and an artificial cell senescence model were established as described.[16] Then, m^{6}A dot blot analysis and m^{6}A quantification analysis were conducted on mice hearts at 3 different ages (3, 12, and 24 months), revealing a significant decrease in global m^{6}A methylation levels at 24 months compared with 3-month-old mice (Figure 1A through 1C). To further validate these findings in an in vitro setting, AC16 cardiomyocytes were subjected to treatment with H_2O_2 or AngII to induce cell senescence. Senescence-associated β-galactosidase staining showed a substantial fraction of AC16 cardiomyocytes exhibiting positive staining (Figure S1A). Both H_2O_2 and AngII treatment led to a concentration-dependent decrease in global m^{6}A modification levels in AC16 cardiomyocytes (Figure S1B). Collectively, these results suggest that aging is associated with decreased m^{6}A RNA methylation in the heart.

To gain insights into how the dynamic m^{6}A methylation is exactly altered in the heart during aging, we analyzed the mRNA and protein expression of 2 major m^{6}A erasers (ALKBH5 and FTO) and 2 major m^{6}A writers (METTL3 and METTL14). As mice aged, we found increased mRNA expression of alkbh5, a decrease in mettl3, and no difference in mettl14 and fto (Figure 1D). In line with mRNA expression pattern, ALKBH5 protein expression in the heart increased with age, whereas METTL3, METTL14, or FTO protein expression did not show significant changes (Figure 1E and 1F). These results suggested that the aging-induced upregulation of ALKBH5 may contribute to the decrease in m^{6}A RNA methylation in the heart.

Considering the possibility that doxorubicin itself might independently affect dynamic m^{6}A methylation, irrespective of the age factor, we measured the m^{6}A methylation level and the expression levels of related enzymes using dot blotting and Western blotting, respectively, with heart tissue samples from young mice treated with doxorubicin or saline. In comparison to the control group, the m^{6}A methylation level increased (Figure S1C), accompanied by increased protein expression of Mettl3 and Mettl14 and decreased FTO protein expression, whereas ALKBH5 expression remained unchanged in the hearts of young mice treated with doxorubicin (Figure S1D). These findings suggested that ALKBH5-m^{6}A modification might not be involved in doxorubicin-induced apoptosis in the heart of young mice and further underscore the potential functional importance of specific ALKBH5-m^{6}A regulation during aging in the context of doxorubicin-induced cardiotoxicity.

To further explore the impact of sex differences on RNA m^{6}A modification during aging, we treated human cardiomyocytes (AC16 cells) with β-estradiol for 24 hours before subjecting them to high concentrations of H_2O_2 to establish an artificial cell senescence model. Subsequently, we assessed m^{6}A methylation levels and the expression of related enzymes using dot blotting and Western blotting, respectively. Interestingly, our data revealed no significant difference in m^{6}A methylation levels between the control group and the β-estradiol-treated group, both with and without H_2O_2 treatment, suggesting that estrogen might not affect m^{6}A methylation in AC16 cells during aging (Figure S2A). However, β-estradiol treatment partially reduced the expression level of the senescence marker P21 protein and changed the protein expression levels of m^{6}A-related enzymes (Figure S2B). These in vitro data showed that sex factor, at least in the context of estrogen, may not be involved in ALKBH5-m^{6}A regulation in aging-associated doxorubicin-induced cardiotoxicity. Consequently, for all subsequent in vivo experiments, male mice were exclusively used.

Overexpression of ALKBH5 Deteriorates Doxorubicin-Induced Cardiac Dysfunction and Remodeling in Young Mice

To investigate the potential functional role of ALKBH5 in cardiomyocytes, we employed an AAV9

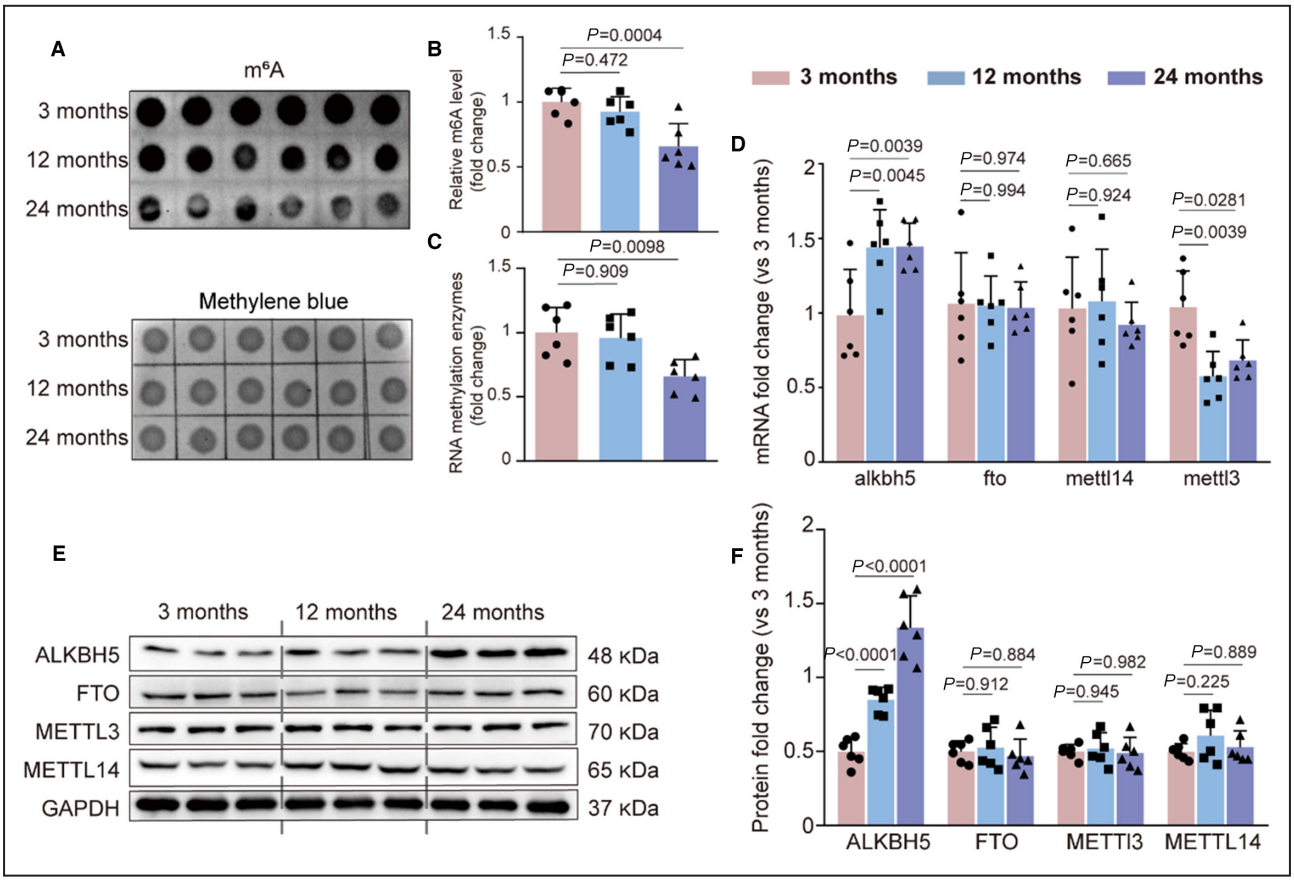

Figure 1. The global m^{6}A methylation level decrease during the aging process resulting from an increase in ALKBH5 protein expression.

A and **B**, m^{6}A dot blot analysis and quantification of m^{6}A in total RNAs from heart tissues of mice at 3 different ages (3, 12, and 24 months, n=6/group). Methylene blue was used as a loading control. **C**, The global m^{6}A methylation level in heart RNA samples was measured using EpiQuik m^{6}A RNA Methylation Quantification Kit (n=6). **D**, Heart mRNA expression of 4 major m^{6}A-related enzymes, including alkbh5, fto, mettl3, and mettl14. **E** and **F**, The heart protein levels of METTL14, METTL3, FTO, and ALKBH5 in mice at 3 different ages (3, 12, and 24 months, n=6). Error bars represent SEM. Data in **B** and **C** were analyzed by 2-way ANOVA with Dunnett's multiple comparisons test, and data in **D** and **F** were analyzed by 2-way ANOVA with Dunnett's multiple comparisons test. ALKBH5 indicates AlkB homolog 5; FTO, fat mass and obesity-associated gene; m^{6}A, N6-methyladenosine; METTL14, methyltransferase 14; and METTL3 methyltransferase 14.

vector containing the cardiac-specific cTnT promoter to achieve specific overexpression of ALKBH5 in the hearts of young mice (3 months) subjected to doxorubicin treatment, as described previously (Figure 2A). Three weeks after viral injection, we observed an increase in both ALKBH5 mRNA and protein levels in the heart (Figure 2B), accompanied by a decrease in m^{6}A modification levels of heart mRNAs (Figure 2C). Notably, mice treated with AAV9-vector or AAV9-ALKBH5 exhibited higher green fluorescence intensity in the hearts, indicating efficient transfection (Figure 2D).

Measurement of body weight revealed no significant changes between the control group and mice overexpressing ALKBH5 (Figure S3A), indicating that cardiac-specific ALKBH5 overexpression did not directly affect body weight. Similarly, no discernible alterations in cardiac function were observed between the control group and ALKBH5 overexpressing mice. However, compared with the AAV9-vector group treated with doxorubicin, the group with ALKBH5 overexpression demonstrated a more pronounced reduction in ejection fraction and fractional shortening (Figure 3A through 3C). This decline in cardiac function was accompanied by a significant elevation in plasma levels of cTnT and creatine kinase-MB isoenzyme as indicators of cardiac injury (Figure S3B and S3C), as well as increased ANP (myocardial atrial natriuretic hormone) and BNP (B-type natriuretic peptide) mRNA levels (Figure S3D and S3E) in the AAV9-ALKBH5 group following doxorubicin treatment.

No significant difference was found between AAV9-vector and AAV9-ALKBH5 groups in cardiac atrophy, cardiac fibrosis, and apoptosis. Following doxorubicin

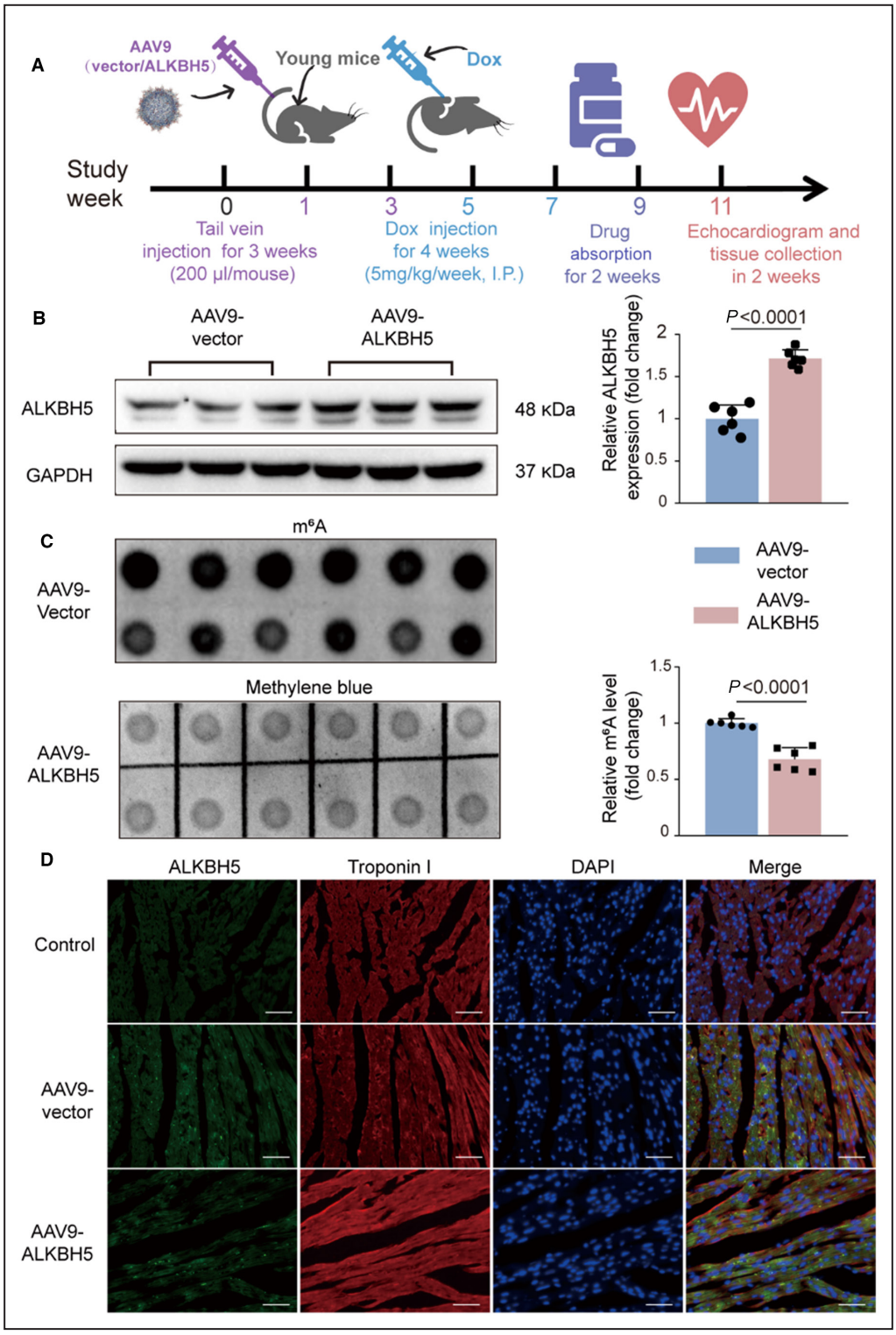

Figure 2. Heart-specific ALKBH5 overexpression in young mice via AAV9.
A, A Schematic of the time in which young mice were injected with AAV9 via tail vein and then intraperitoneally administrated with doxorubicin or saline. **B**, Immunoblotting analysis and quantification of ALKBH5 in hearts from AAV9-vector control (AAV9-vector) or AAV9-ALKBH5 overexpression (AAV9-ALKBH5) mice. n=6. **C**, m^{6}A dot blot analysis and quantification of m^{6}A in total RNAs from heart tissues of AAV9-vector or AAV9-ALKBH5 mice. Methylene blue staining was used as a loading control. n=6. **D**, Representative images of eGFP, troponin I, and DAPI fluorescence of histological sections of hearts from AAV9-vector and AAV9-ALKBH5 treated mice. Scale bars=100 μm. Error bars represent SEM. Data were analyzed by unpaired 2-tailed Student *t* test. AAV indicates adeno-associated viruses; ALKBH5, AlkB homolog 5; Dox, doxorubicin; eGFP, enhanced green fluorescent protein; and m^{6}A, N6-methyladenosine.

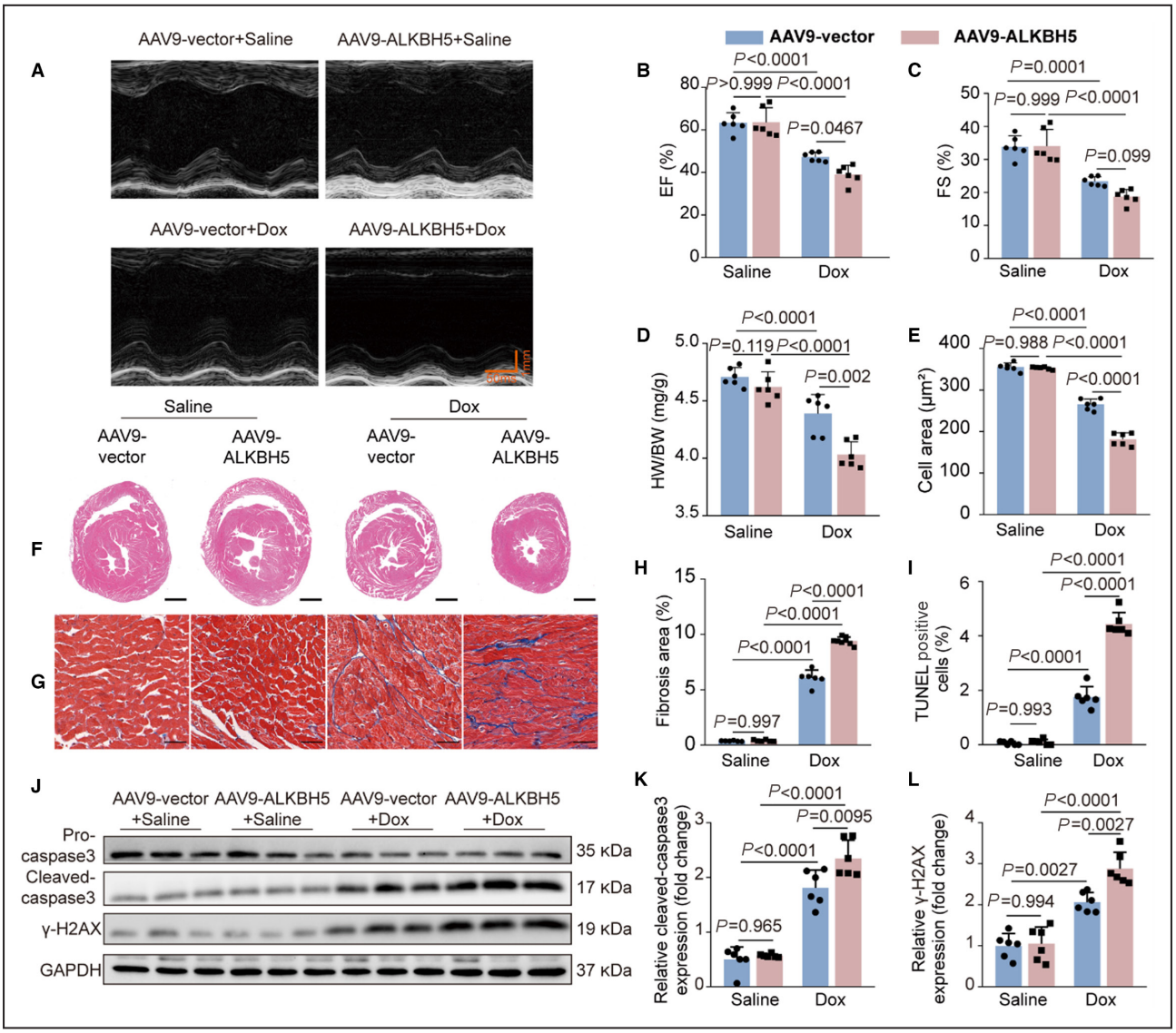

Figure 3. Heart-specific overexpression of ALKBH5 deteriorates doxorubicin-induced left ventricular dysfunction, cardiac remodeling, and cardiomyocyte apoptosis in young mice.
A, Sample M-mode short-axis echocardiographic images for evaluating heart function by echocardiography analysis between weeks 11 and 12. **B** and **C**, EF% and FS% of mice as determined via echocardiography 2 weeks after doxorubicin injection. n=6. **D**, Statistical results of the HW/BW. n=6. **E**, Statistical results of cardiomyocyte size assessment. n=6. **F**, Representative images of the heart cross-sections with hematoxylin–eosin staining. Scale bars: 1 mm. **G**, Representative images of fibrosis by Masson trichrome staining hearts after doxorubicin treatment. n=6. Scale bar: 20 μm. **H**, Relative quantification of collagen deposition in Masson trichrome stained heart sections. n=6. **I**, Quantification of TUNEL staining for apoptosis in heart sections. n=6. **J**, Immunoblotting analysis of pro-caspase3, cleaved-caspase3, and γ-H2AX protein expression. **K**, Statistical results of cleaved-caspase3 activation. n=6. L, Statistical results of γ-H2AX protein expression. n=6. Error bars represent SEM. Data were analyzed by 2-way ANOVA, followed by the Tukey post hoc test. AAV indicates adeno-associated viruses; ALKBH5, AlkB homolog 5; Dox, doxorubicin; EF%, ejection fraction; FS%, fractional shortening; HW/BW, heart weight/body weight length; TUNEL, terminal deoxynucleotidyl transferase dUTP nick end labeling; and γ-H2AX, phospho-histone H2A.X.

treatment, ALKBH5-overexpressing mice exhibited decreased relative heart weight (Figure 3D; Figure S3F and S3G), heart cross-sectional area (Figure 3F), and cardiomyocyte cell size (Figure S3H; Figure 3E) compared with the AAV9-vector mice. Conversely, ALKBH5-overexpressing mice demonstrated increased cardiac interstitial fibrosis, as evidenced by Masson trichrome staining (Figure 3G and 3H), higher levels of apoptosis indicated by more TUNEL-positive cells (Figure S3I; Figure 3I), intensified activation of cleaved-caspase3 (Figure 3J and 3K), and elevated DNA damage represented by increased γ-H2AX expression (Figure 3J and 3L). These collective findings suggest that heart-specific ALKBH5 overexpression does not adversely

affect cardiac function, structure, and cell viability but significantly exacerbates doxorubicin-induced cardiac dysfunction, atrophy, and cardiomyocyte damage.

ARID2 Is Regulated by ALKBH5-Mediated m^{6}A Modification in Cardiomyocytes

To elucidate the molecular targets influenced by ALKBH5-mediated m^{6}A modification in cardiomyocytes, we conducted N6-methyladenosine-sequencing and RNA sequencing analyses using ALKBH5-overexpressing AC16 cardiomyocytes. By comparing the results to control samples, we identified 67 genes that overlapped between 847 m^{6}A-regulated genes (with a fold change >2.0 in m^{6}A modification) and 635 significantly upregulated or downregulated mRNAs in response to ALKBH5 overexpression (Figure 4A and 4B).

Then, we further narrowed the potential target genes based on log2FC<–2 in m^{6}A modification and log2FC < –1 in expression differences. Interestingly, among these genes, ARID2, which is associated with DNA damage repair, ranked ninth as one of the most significantly downregulated genes (Figure 4C). ARID2, a subunit of the PBAF (polybromo-associated BAF) complex, has previously been implicated in heart morphogenesis and coronary artery angiogenesis (Figure 4D), suggesting its potential involvement in the progression of heart failure. Notably, analysis using an integrative genomics viewer revealed a prominent m^{6}A peak located in exon 15 of the ARID2 gene (Figure 4E), which was enriched in the m^{6}A consensus motif RRACH (Figure 4F). The predicted m^{6}A modification sites of ARID2 mRNA were listed in Figure S4A.

To further confirm that ARID2 mRNA undergoes ALKBH5-mediated m^{6}A methylation and to identify the major m^{6}A modification sites identified through m^{6}A sequencing, we performed MeRIP-PCR using specific primers (detailed sequences in Table S1). The data indicated that ARID2 mRNA degradation occurred following a decline in m^{6}A methylation induced by ALKBH5 overexpression (Figure 4G). Moreover, both primers set 1 and 2 revealed potential m^{6}A motifs, suggesting the presence of methylation modification binding sites on ARID2.

Next, we further verified the exact m^{6}A motif by luciferase activity assay after ALKBH5 silence. The pnirGLO-ARID2-WT luciferase reporter containing ARID2 3'UTR after the firefly luciferase coding sequence was synthesized, and thymine bases were substituted for the adenosine bases in the m^{6}A motif sequences to establish 3 pmirGLO-ARID2-MUT luciferase reporters (Figure 4H). The data showed a marked rise of luciferase activity upon ALKBH5 knockdown in pmirGLO-ARID2-WT and pmirGLO-ARID2-MUT2&3 groups, whereas pmirGLO-ARID2-MUT1 showed no response to ALKBH5 knockdown (Figure 4I). These results revealed that the regulation of ARID2 expression was controlled by ALKBH5-mediated m^{6}A modification on the ARID2 3′ UTR at motif 1.

To identify the responsible m^{6}A reader for ARID2 expression, we knocked down 5 known m^{6}A readers, including YTHDC1–2 and (YTHDF1–3, using siRNA in AC16 cells transfected with pmirGLO-ARID2-WT or pmirGLO-ARID2-MUT1 (Figure 4J; Figure S4B). Following YTHDF1 knockdown, the luciferase activity of pmirGLO-ARID2-WT significantly decreased, and pmirGLO-ARID2-MUT1 showed no response to YTHDF1 knockdown. Together, these findings suggest that YTHDF1 contributes to the regulation of ALKBH5-mediated m^{6}A modified ARID2 mRNA decay and further confirms the specific m^{6}A motif.

Next, we further explored the biological function of ALKBH5-mediated m^{6}A modification in ARID2 mRNA metabolism with actinomycin D in AC16 cells. The results showed that the loss of m^{6}A modification by overexpressing ALKBH5 resulted in a more significant degradation rate of ARID2 mRNA, which was verified by RNA stability assay (Figure S4C).

Furthermore, we evaluated how aging affected ARID2 expression in vitro. The aging-related ARID2 downregulation was further validated using quantitative RT-PCR (Figure S4D) and Western blot. Notably, ALKBH5 overexpression led to a reduction in ARID2 expression, whereas ALKBH5 silencing resulted in enhanced ARID2 protein expression (Figure 4K and 4L). These findings indicate that ARID2 expression decreases with aging and is regulated by ALKBH5.

ARID2 Improves Doxorubicin-Induced Cardiomyocytes Apoptosis Via Modulating DNA Damage Response

Given that ARID2 is known to modulate DNA damage repair,[17] we sought to investigate the potential correlation between ARID2 expression and doxorubicin-induced cardiomyocyte death. ARID2 functions as a subunit of the PBAF chromatin remodeling complex, along with 2 other subunits, PBRM1 and BRD7. Notably, we observed a consistent pattern of changes in protein levels of ARID2, PBRM1, and BRD7 upon silencing and overexpressing ARID2 in vitro (Figure S4E and S4F). These findings suggest that ARID2 may play a crucial role in maintaining the stability of PBAF-specific subunits.

To further elucidate the role of ARID2 and its downstream target genes (PBRM1 and BRD7) in the context of aging, ALKBH5 expression, and doxorubicin treatment, we examined the protein levels of ARID2, PBRM1, and BRD7 in mouse hearts. We observed a decrease in the expression of ARID2, PBRM1, and BRD7 in hearts from old mice, doxorubicin-treated mice, and ALKBH5-overexpressing young mice (Figure S5A through S5C). This decrease in expression

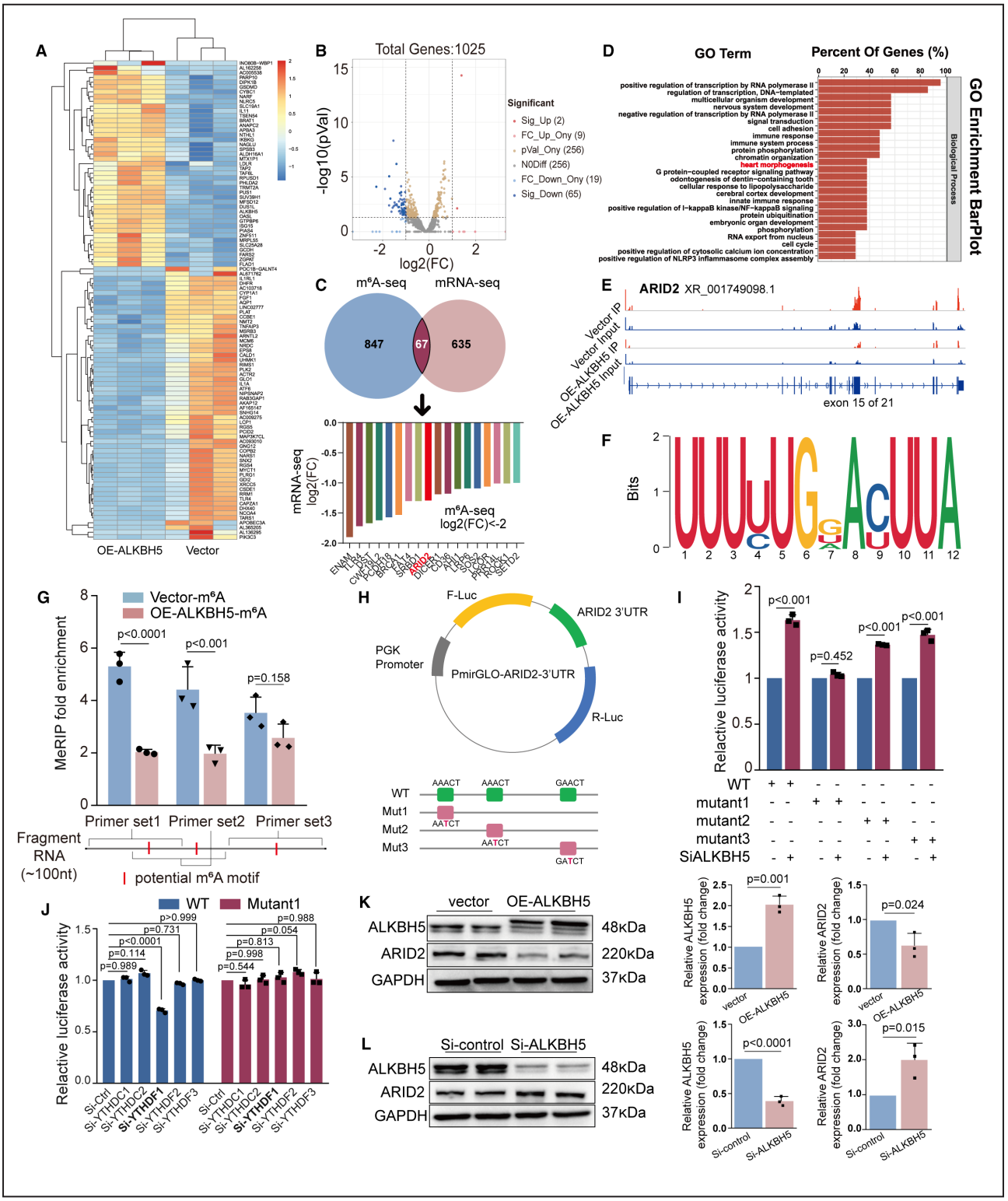

suggests a potential decline in the efficiency of DNA damage repair mechanisms.

To assess the potential correlation between ARID2 expression and doxorubicin-induced cardiomyocyte death, we treated AC16 cardiomyocytes with doxorubicin to induce apoptosis and evaluated apoptosis levels using TUNEL staining to detect DNA fragmentation. Interestingly, ARID2 silencing aggravated doxorubicin-induced apoptosis (Figure S6A and S6B), whereas ARID2 overexpression attenuated doxorubicin-induced apoptosis (Figure S6C and S6D). Conversely, ALKBH5 overexpression increased doxorubicin-induced

Figure 4. ARID2 is regulated by ALKBH5-mediated m^{6}A modification in cardiomyocytes.
A, Heatmap showing differentially expressed mRNAs in lentiviral transfection of ALKBH5-overexpression or empty vector AC16 cells (n=3 of each group). **B**, Volcano plots showing differentially m^{6}A-modified mRNAs based on |log2FC|>1 and *P* value<0.05. **C**, A Venn diagram of m^{6}A modified genes in lentiviral transfection of ALKBH5-overexpression or empty vector AC16 cells and the list of overlap genes was ranked based on log2FC<–2 in m^{6}A modification and log2FC<–1 in expression differences. **D**, GO enrichment analysis of differential genes upon ALKBH5 overexpression. **E**, Distribution of m^{6}A peaks across arid2 mRNA transcripts. **F**, Sequence motif identified within m^{6}A peaks across arid2 mRNA transcripts. **G**, m^{6}A modification of ARID2 mRNA was analyzed by MeRIP-quantitative polymerase chain reaction. **H**, WT or m^{6}A consensus sequence mutant ARID2-3′UTR was fused with a firefly luciferase reporter. Mutation of m^{6}A consensus sequences was generated by replacing adenosine with thymine. n=3. **I**, Relative luciferase activity of the WT and 3 mutant ARID2-3′UTR reporter vectors in AC16 cells transfected with control siRNA or siRNA targeting ALKBH5. n=3. **J**, Relative luciferase activity of the WT and ARID2-mutant AC16 cells transfected with control siRNA or siRNA targeting YTHDC1, YTHDC2, YTHDF1, YTHDF 2, and YTHDF 3. n=3. **K**, Immunoblotting analysis and quantification of ALKBH5 and ARID2 in AC16 cells transfected with ALKBH5-overexpression plasmid or vector. n=3. **L**, Immunoblotting analysis and quantification of ALKBH5 and ARID2 in AC16 cells transfected with control siRNA or siRNA targeting ALKBH5. n=3. Error bars represent SEM. Two-way ANOVA with Tukey post hoc test was used for data analysis in **G**, **I**, and **J**, and unpaired 2-tailed Student *t* test was used for data analysis in **K** and **L**. ALKBH5 indicates AlkB homolog 5; ARID2, AT-rich interaction domain 2; Ctrl, control; F-luc, firefly luciferase; GO, Gene Ontology; m^{6}A, N6-methyladenosine; MeRIP, m^{6}A-RNA Immunoprecipitation; OE, overexpression; R-luc, renilla luciferase; seq, sequencing; siRNA, small interfering RNA; WT, wild type mice; YTHDC1–2, YTH domain-containing family protein; and YTHDF1–3, YTH N6-methyladenosine RNA binding family protein.

apoptosis (Figure S6E and S6F). Intriguingly, the double overexpression of ALKBH5 and ARID2 significantly decreased doxorubicin-induced apoptosis compared with the ALKBH5-overexpression group treated with doxorubicin (Figure 5A and 5B). These results suggest that ALKBH5 overexpression exacerbates doxorubicin-induced cardiomyocyte apoptosis, while ARID2 overexpression counteracts the effect of ALKBH5 overexpression in doxorubicin-induced cardiomyocyte apoptosis.

To monitor DNA damage and repair, we assessed the expression of γ-H2AX, a biomarker of cellular response to DNA double-strand break repair. In AC16 cardiomyocytes overexpressing ALKBH5 and treated with doxorubicin for 12 hours, γ-H2AX expression increased compared with the nontreatment group (Figure S6G and S6H). Following the removal of doxorubicin from the medium, the γ-H2AX level gradually decreased over time in both the vector and ALKBH5-overexpressing groups. However, between 0 and 8 hours, the ALKBH5-overexpressing group exhibited higher γ-H2AX expression compared with the vector group. Consistent with the TUNEL staining results, the double overexpression of ARID2 and ALKBH5 significantly reduced the number of γ-H2AX foci (Figure 5C and 5D) and γ-H2AX expression (Figure 5E and 5F) at the indicated time points (0, 4, and 8 hours) compared with the group with ALKBH5 overexpression alone.

Together, these findings collectively suggest that ALKBH5-mediated m^{6}A modification contributes to doxorubicin-induced cardiomyocyte apoptosis, which could be further aggravated by regulating DNA damage repair processes.

Knockdown of ALKBH5 Mitigates Doxorubicin-Induced Cardiac Dysfunction and Remodeling in Old Mice

Up to this point, the aforementioned findings have provided compelling evidence of the exacerbating effect of ALKBH5 overexpression on doxorubicin-induced cardiotoxicity in young mice. In light of these results, we sought to investigate whether specific knockdown of ALKBH5 in cardiomyocytes could ameliorate the detrimental effects of doxorubicin treatment in old mice (20 months). Accordingly, we generated cardiac-selective AAV9-shRNA with the presence of the cTnT promoter to knock down ALKBH5 in old mice (Figure S7A). As expected, the expression levels of ALKBH5 mRNA and protein (Figure S7B and S7C) in heart tissues were significantly reduced, whereas m^{6}A RNA methylation (Figure S7D and S7E) increased 4 weeks after AAV9-shALKBH5 injection. Fluorescence imaging of the heart demonstrated high transfection efficiency in mice treated with AAV9-shctrl or AAV9-shALKBH5, as indicated by the elevated fluorescence intensity (Figure S7F). Mechanistically, we observed an upregulation in the protein expression of ARID2, PBRM1, and BRD7 in the cardiac tissue of old mice with ALKBH5 knockdown compared with the corresponding control group (Figure S8). This observation suggests a potential recovery in the DNA damage repair ability in response to ALKBH5 suppression during aging.

No significant changes in body weight were found among mice (Figure S9A), suggesting heart-specific knockdown of ALKBH5 had no direct effect on body weight. Similarly, no significant changes were found between AAV9-shctrl and AAV9-shALKBH5 mice in cardiac function. However, compared with the old mice treated with doxorubicin, the knockdown of ALKBH5 significantly mitigated doxorubicin-induced cardiac dysfunction in old mice as indicated by increased ejection fraction and fractional shortening (Figure 6A through 6C), reduced levels of serum cTnT and creatine kinase MB isoenzyme (Figure S9B and S9C), and downregulated expression of ANP and BNP mRNA (Figure S9D and S9E). Notably, no significant differences were observed in terms of cardiac atrophy, cardiac fibrosis, and apoptosis between the

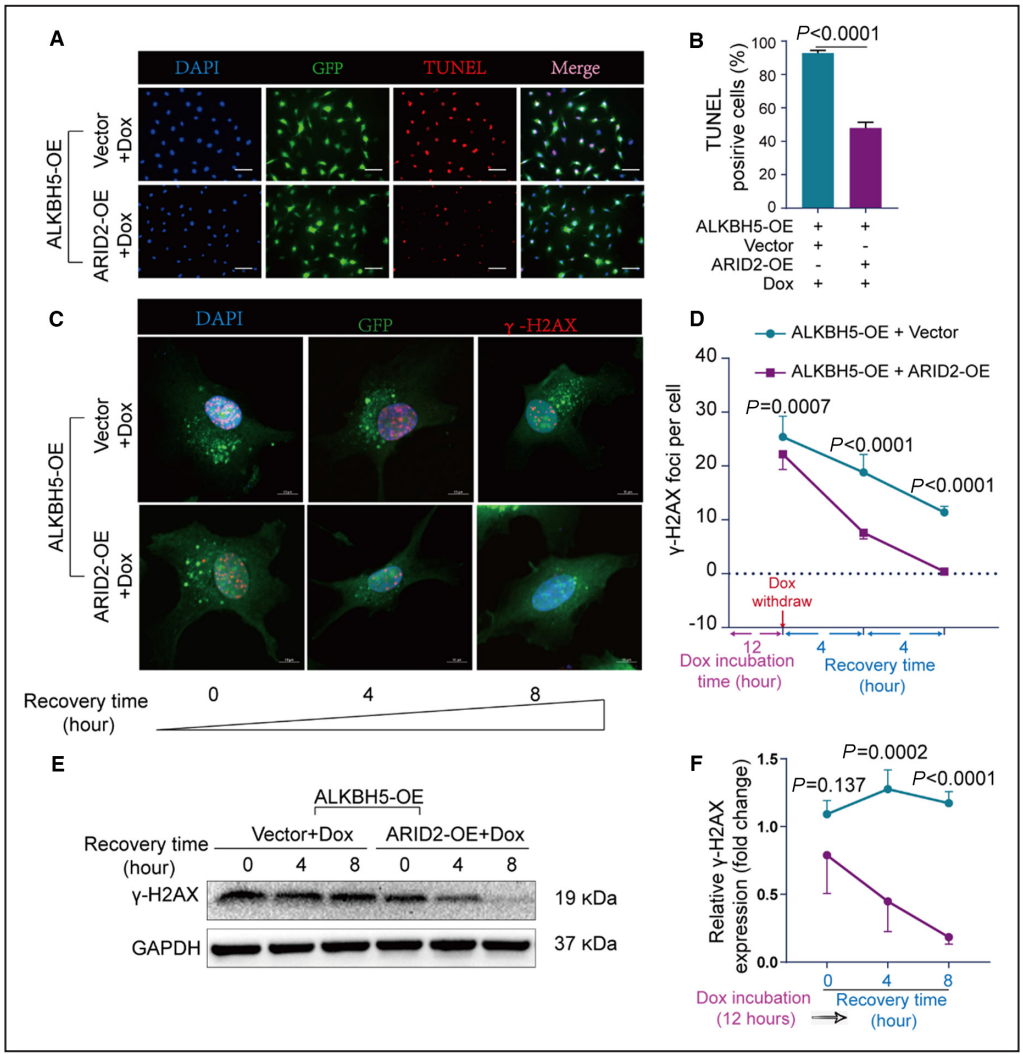

Figure 5. ARID2 protects cardiomyocytes from doxorubicin-induced apoptosis via modulating DNA damage response.

A and **B**, Representative images and analysis of combined ALKBH5 and ARID2-overexpression AC16 cardiomyocytes with the treatment of doxorubicin (0.5 μmol/L) via TUNEL staining (red). Scale bar: 100 μm. n=4 different fields from 3 different experiments per group. **C** and **D**, Representative images and quantification analysis of DNA-repair foci visualized by γ-H2AX immunofluorescence (red) in transduced nuclei stained with DAPI (blue) at different recovery times after the treatment of doxorubicin (0.5 μmol/L) in combined ALKBH5 and ARID2-overexpression and only ALKBH5-overexpression AC16 cardiomyocytes. Scale bar: 10 μm. n=4 different fields from 3 different experiments per group. **E** and **F**, Immunoblotting analysis and quantification of γ-H2AX proteins in combined ALKBH5 and ARID2-overexpression and only ALKBH5-overexpression AC16 cardiomyocytes at the indicated time points after removing doxorubicin from the medium. n=3. Error bars represent SEM. Unpaired 2-tailed Student *t* test was used for data analysis in **B**, and 2-way ANOVA with Sidak's multiple comparisons test was used for data analysis in **D** and **F**. ALKBH5 indicates AlkB homolog 5; ARID2, AT-rich interaction domain 2; GFP, green fluorescent protein; OE, overexpression; TUNEL, terminal deoxynucleotidyl transferase dUTP nick end labeling; and γ-H2AX, phospho-histone H2A.X.

control and ALKBH5-knockdown mice. However, relative heart weight (Figure 6D; Figure S9F and S9G), heart cross-sectional area (Figure 6F), and cardiomyocyte cell size (Figure S9H; Figure 6E) were found to be increased in ALKBH5-knockdown mice compared with the AAV9-shctrl mice post doxorubicin treatment. Meanwhile, less cardiac interstitial fibrosis, as shown by Masson trichrome staining (Figure 6G and 6H), decreased levels of apoptosis, with fewer TUNEL-positive cells (Figure S9I; Figure 6I), and reduced activation of cleaved caspase-3 (Figure 6J and 6K) and DNA damage, as denoted by lower γ-H2AX expression (Figure 6J and 6L), were observed in heart-specific ALKBH5-knockdown mice following

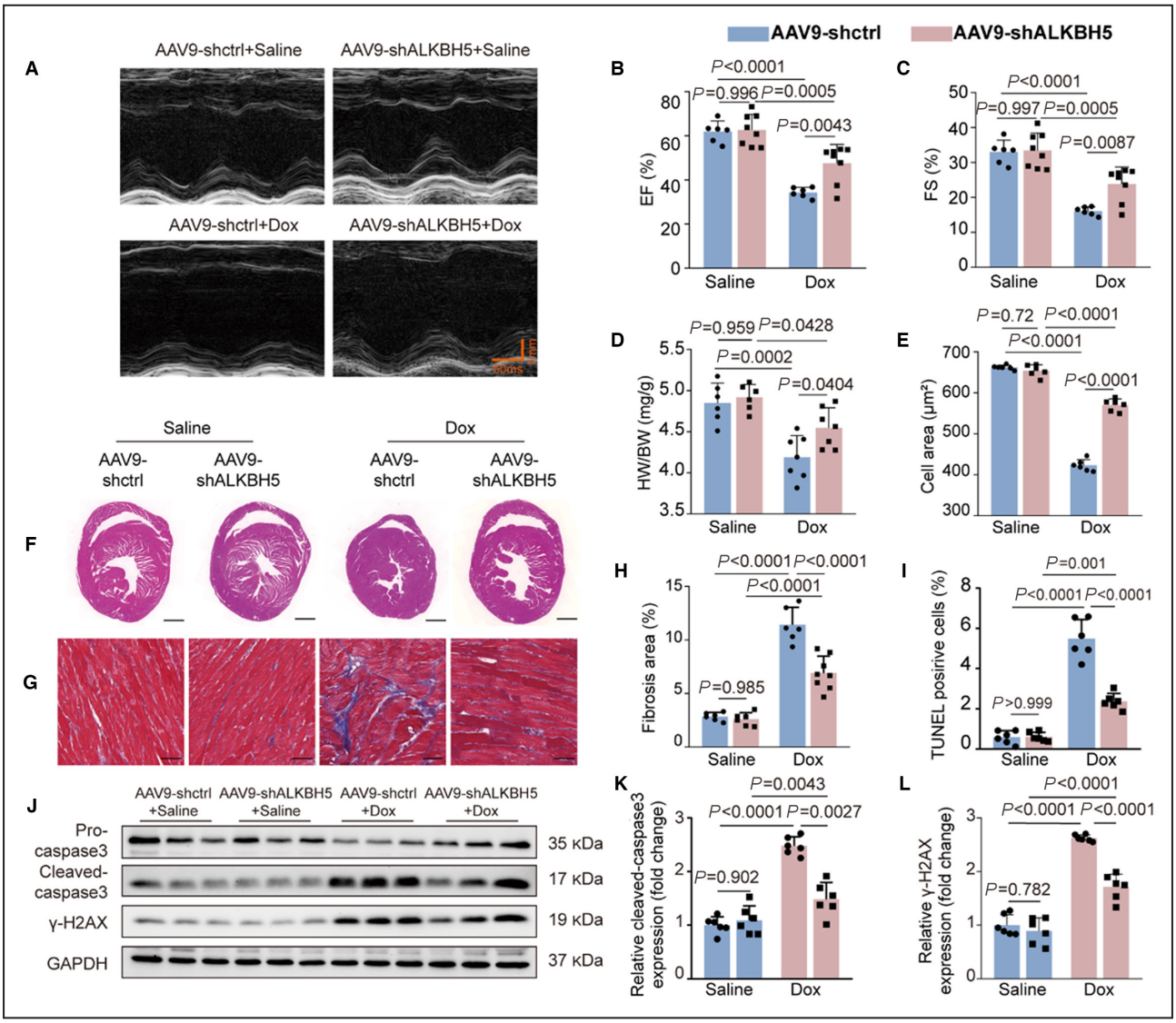

Figure 6. Heart-specific downregulation of ALKBH5 improves doxorubicin-induced left ventricular dysfunction, cardiac remodeling, and cardiomyocyte apoptosis in old mice via AAV9.

A, Sample M-mode short-axis echocardiographic images for evaluating heart function by echocardiography analysis between weeks 11 and 12. **B** and **C**, EF%, and FS% of mice as determined via echocardiography 2 weeks after doxorubicin injection. n=6. **D**, Statistical results of the HW/BW. n=6. **E**, Measurement of cardiomyocyte size in the hematoxylin–eosin-stained heart sections. n=6. Scale bar: 20 μm. **F**, Representative images of the heart cross-sections with hematoxylin–eosin staining. Scale bars: 1 mm. **G**, Representative images of fibrosis by Masson trichrome staining hearts after doxorubicin treatment. n=6. Scale bar: 20 μm. **H**, Relative quantification of collagen deposition in Masson trichrome stained heart sections. n=6. **I**, Quantification of TUNEL staining for apoptosis in heart sections. n=6. **J**, Immunoblotting analysis of pro-caspase3, cleaved-caspase3, and γ-H2AX protein expression. **K**, Statistical results of cleaved-caspase3 activation. n=6. **L**, Statistical results of γ-H2AX protein expression. n=6. Error bars represent SEM. Data were analyzed by 2-way ANOVA, followed by the Tukey post hoc test. AAV indicates adeno-associated viruses; ALKBH5 indicates AlkB homolog 5; Ctrl, control; Dox, doxorubicin; EF%, ejection fraction; FS%, fractional shortening; HW/BW, heart weight/body weight length; TUNEL, terminal deoxynucleotidyl transferase dUTP nick end labeling; and γ-H2AX, phospho-histone H2A.X.

doxorubicin treatment, in comparison to old mice treated with doxorubicin.

Taken together, these results suggest that while ALKBH5 knockdown alone in old mice did not confer beneficial effects on cardiac function, structure, and cell viability, it significantly alleviated doxorubicin-induced cardiac dysfunction, atrophy, and cardiomyocyte damage.

Considering the focus of our study on doxorubicin-induced cardiomyocyte apoptosis, it is essential to ensure that any interventions employed do not compromise the efficacy of oncological therapy. To elucidate the involvement of ALKBH5 in cancer cells, particularly MCF-7 breast cancer cells, we conducted an EDU staining assay. Our results demonstrate that ALKBH5 knockdown

significantly suppressed the proliferation of breast cancer cells (Figure S10A and S10B). Additionally, when MCF-7 cells were treated with a lower dose of doxorubicin (0.125 μmol/L), a notable increase in cell death was observed compared with control cells (Figure S10C), along with impaired colony formation (Figure S10D). Collectively, these findings indicate that ALKBH5 inhibition impedes the progression of breast cancer cells, highlighting its potential as a therapeutic target.

DISCUSSION

Cancer is increasing in incidence and prevalence with the increased aging of the population.[3,18] Recent studies showed that patients 65 years of age and older with cancer were more likely to have a higher rate of chemotherapy-related cardiotoxicity than young patients.[19,20] Unfortunately, the pathogenic mechanism of chemotherapy-induced cardiotoxicity is unclear, and reliable biomarkers and treatment for elderly patients with cancer are limited.

In this study, we used young and old mice administered with doxorubicin to mimic the pattern of DIC progression in young and older humans. According to the guidelines of cardioncology, myocardial dysfunction and heart failure are typical clinical signs of chemotherapy-induced cardiotoxicity in patients with cancer,[21,22] so transthoracic echocardiography, serum cardiac markers, the cardiac natriuretic peptides, heart weight, and cross-sections with indicated staining were used to assess the change in function and structure of the heart. Consistent with findings in previous studies, doxorubicin causes heart failure in young mice, whereas all the biochemical indicators of heart failure mentioned were more pronounced in old mice. These results verified the susceptibility of old mice to doxorubicin-induced cardiac dysfunction. Besides the loss of body weight caused by doxorubicin, cardiac atrophy and myocardial cell loss can also occur,[23] because doxorubicin caused a decrease in cardiac protein synthesis.[24] Notably, we observed a reduction in the weight of the whole heart and its cardiomyocyte sizes in doxorubicin-treated mice. This result is consistent with other recent experimental studies,[23,25] which demonstrated that reduced left ventricular mass, increased levels of interstitial fibrosis, and reduced cardiomyocyte size are involved in the early and subclinical myocardial effects of anthracycline-induced cardiotoxicity. More important, our data illustrated aging caused doxorubicin-induced cardiotoxicity deterioration in old mice, manifested by lower fractional shortening and cardiomyocyte contraction, higher biomarkers of myocardial injury, smaller cardiomyocyte size, more myocardial fibrosis, and more apoptotic cardiomyocytes. Even though the aging process has long been recognized as an independent risk factor of DIC,[3] the detailed mechanisms linking them remain to be determined yet.

Abnormal m^{6}A modification has been shown to regulate diverse cellular processes and cause impaired embryonic development,[26] tumorigenesis,[27] age-related neurodegenerative disorders,[28] age-related infertility, and heart failure,[9,29] etc. These findings highly suggest that m^{6}A RNA methylation may be the link between aging and DIC. Here, we found the globe m^{6}A RNA methylation level was deregulated and only its demethylase ALKBH5 protein level was upregulated in the heart of old mice, indicating ALKBH5 might contribute to the aging-associated m^{6}A RNA methylation downregulation in the heart. In recent studies, dysregulation of m^{6}A methylation is also regarded as a hallmark of mammalian heart failure.[5–7,9] Their data showed increased m^{6}A RNA methylation in failing hearts and hypoxic cardiomyocytes because of different HF model establishment methods, different effector enzymes, or different mice with varying ages.

To further verify whether ALKBH5-derived m^{6}A RNA methylation change modulated aging-associated DIC, we used an AAV9-mediated overexpression system for heart-specific ALKBH5 overexpression and knockdown in young mice and old mice, respectively. We detected a strong exacerbation effect of ALKBH5 overexpression in doxorubicin-induced cardiac dysfunction and structural abnormalities, which were consistent with the observed changes in aging-associated DIC. Furthermore, ALKBH5 knockdown markedly alleviated the doxorubicin-induced cardiac dysfunction and structural abnormalities in aging mice. These results suggested ALKBH5 modulated doxorubicin-induced cardiac dysfunction during aging. Downregulation of ALKBH5-mediated m^{6}A demethylation serves a therapeutic role in aging-associated DIC, which laid the groundwork for future clinical translation of a therapy to treat aging-associated DIC.

This led us to investigate whether ALKBH-m^{6}A methylation modulated some specific subsets of mRNAs correlated with cardiomyocyte apoptosis. Genome-wide m^{6}A-sequencing and mRNA-sequencing analysis in ALKBH5-overexpressed cardiomyocytes represented the first ALKBH5 overexpression in cardiomyocytes. Among those mRNA expression-altered genes with m^{6}A downregulation, the top-ranked gene ARID2 related to the DNA damage repair was identified as a potential effector of ALKBH5 in DIC. Meanwhile, we also identified the specific modification loci and YTHDF1 as coregulator of ALKBH5-m^{6}A modification. Previous studies demonstrated doxorubicin can intercalate into

nuclear DNA and inhibit the progression of topoisomerase II, resulting in DNA damage.[30,31] The deficiency of ARID2, a component of the BAF chromatin remodeling complex, had been proved to inhibit DNA repair[32] and attenuate nucleotide excision repair of DNA damage sites,[33] resulting in susceptibility to carcinogens and potential hypermutation[33] but sensitivity enhancement to chemotherapy in lung cancer cells.[32] In addition, ARID2 plays a pivotal role in heart morphogenesis and coronary artery angiogenesis.[34] Notably, it was indicated other components of the BAF complex were linked to the process of myocardial hypertrophy,[35] cardiac reprogramming,[36] cardiomyocyte cell fate,[37] cardiac arrhythmias,[38] and heart developing.[39] Furthermore, ARID2 was reported to be a coregulatory of other PBAF complex members in some clonal cell lines in a recent study,[40] which was also supported by our in vivo and in vitro data. Next, we found ALKBH5 overexpression aggravated doxorubicin-induced cardiomyocyte apoptosis, which could be reversed by further ARID2 overexpression via, at least in part, enhancing DNA damage repair. Collectively, ARID2 is an important downstream target of the ALKBH5-m^{6}A effect in doxorubicin-induced cardiomyocyte apoptosis by modulating the DNA damage repair process.

The primary purpose of doxorubicin treatment is to kill the tumor cells. Despite the specific mechanisms of m^{6}A involved in different tumor progressions remaining elusive,[41] downregulation of ALKBH5-mediated m^{6}A demethylation treatment merits consideration, especially for patients with cancer and ALKBH5-mediated adverse effect on tumor progression or sensitivity to the chemotherapy.[42,43] Thus, we also provided evidence that the silence of ALKBH5 promoted apoptosis and prevent the progression of MCF-7 breast cancer cells.

We acknowledge 3 major limitations of this study. First, we used the AC16 cardiomyocytes for all in vitro experiments, but the primary cardiomyocytes isolated from mice hearts should be more compelling. Second, the role of ARID2 in doxorubicin-induced cardiomyocyte damage is still worthy of using cardiomyocyte-specific ARID2 overexpression mice for further study. Third, considering estrogen contributed to sex differences in heart disease,[44] female mice were excluded from our experimental plan. Interestingly, a recent study showed no difference in both m^{6}A methylation and ALKBH5 expression in the hearts of young and old female mice.[45] Even though our in vitro data showed no influence of estrogen on the m^{6}A methylation in AC16 cells during aging, we admit that only the estrogen factor could not fully account for the sex difference. Thus, we believe it is necessary to further explore the effect of sex differences on aging-related diseases in future follow-up studies.

CONCLUSIONS

In summary, our study provides valuable insights into the molecular mechanism in posttranscriptional modifications regulating the pathogenesis of aging-associated doxorubicin-induced cardiotoxicity. Moreover, our findings highlight the potential value of ALKBH5-mediated m^{6}A regulation as a promising target for preventive or therapeutic interventions against chemotherapy-induced cardiotoxicity in elderly patients with cancer. These findings hold significant clinical implications and underscore the importance of exploring ALKBH5-m^{6}A regulation as a potential avenue for safeguarding the cardiac health of elderly individuals undergoing cancer treatment.

ARTICLE INFORMATION

Received June 11, 2023; accepted November 20, 2023.

Affiliations

Center for Vascular Disease and Translational Medicine (R.C., G.Z., A.F.C.) and Department of Cardiology (R.C., G.Z., A.F.C.), The Third Xiangya Hospital of Central South University, Changsha, Hunan, Chinaand (K.S., A.F.C.), Institute for Developmental and Regenerative Cardiovascular Medicine, Xinhua Hospital, Shanghai Jiao Tong University School of Medicine, Shanghai, China.

Acknowledgments

We thank Gopinath Sutendra, Yi Niu, Yiping Leng, and Guocheng Huang for their helpful discussion in the article revision process; Jie Zhang for assistance in echocardiography measurement; Jingjing Cai for providing the AC16 cell lines.

Sources of Funding

This work was supported in part by grants from the Ministry of Science and Technology of China (2021YFA0804803 and 2022YFA1104204), the Major Project of Natural Science Foundation of Hunan Province (Open Competition) (2021JC0002), and the National Science Foundation of China (81930012, 82241027, 81720108003, and 82130015). Funders provide financial support for this study. Notably, the funders played no part in the design of the study, data collection, analysis, interpretation, report writing, or the decision to submit the article for publication.

Disclosures

None.

Supplemental Material

Table S1–S2
Figures S1–S10

REFERENCES

1. Aiken MJ, Suhag V, Garcia CA, Acio E, Moreau S, Priebat DA, Chennupati SP, Van Nostrand D. Doxorubicin-induced cardiac toxicity and cardiac rest gated blood pool imaging. *Clin Nucl Med*. 2009;34:762–767. doi: 10.1097/RLU.0b013e3181b7d76f
2. Zhang S, Liu X, Bawa-Khalfe T, Lu LS, Lyu YL, Liu LF, Yeh ET. Identification of the molecular basis of doxorubicin-induced cardiotoxicity. *Nat Med*. 2012;18:1639–1642. doi: 10.1038/nm.2919
3. Hurria A, Levit LA, Dale W, Mohile SG, Muss HB, Fehrenbacher L, Magnuson A, Lichtman SM, Bruinooge SS, Soto-Perez-de-Celis E, et al. Improving the evidence base for treating older adults with cancer: American Society of Clinical Oncology statement. *J Clin Oncol*. 2015;33:3826–3833. doi: 10.1200/JCO.2015.63.0319

4. Huang H, Weng H, Chen J. The biogenesis and precise control of RNA mA methylation. *Trends Genet*. 2020;36:44–52. doi: 10.1016/j.tig.2019.10.011
5. Mathiyalagan P, Adamiak M, Mayourian J, Sassi Y, Liang Y, Agarwal N, Jha D, Zhang S, Kohlbrenner E, Chepurko E, et al. FTO-dependent N-Methyladenosine regulates cardiac function during remodeling and repair. *Circulation*. 2019;139:518–532. doi: 10.1161/CIRCULATIONAHA.118.033794
6. Han Z, Wang X, Xu Z, Cao Y, Gong R, Yu Y, Yu Y, Guo X, Liu S, Yu M, et al. ALKBH5 regulates cardiomyocyte proliferation and heart regeneration by demethylating the mRNA of YTHDF1. *Theranostics*. 2021;11:3000–3016. doi: 10.7150/thno.47354
7. Berulava T, Buchholz E, Elerdashvili V, Pena T, Islam MR, Lbik D, Mohamed BA, Renner A, von Lewinski D, Sacherer M, et al. Changes in m^{6}A RNA methylation contribute to heart failure progression by modulating translation. *Eur J Heart Fail*. 2020;22:54–66. doi: 10.1002/ejhf.1672
8. Gao X-Q, Zhang Y-H, Liu F, Ponnusamy M, Zhao X-M, Zhou L-Y, Zhai M, Liu C-Y, Li X-M, Wang M, et al. The piRNA CHAPIR regulates cardiac hypertrophy by controlling METTL3-dependent N-methyladenosine methylation of Parp10 mRNA. *Nat Cell Biol*. 2020;22:1319–1331. doi: 10.1038/s41556-020-0576-y
9. Dorn LE, Lasman L, Chen J, Xu X, Hund TJ, Medvedovic M, Hanna JH, van Berlo JH, Accornero F. The N-Methyladenosine mRNA Methylase METTL3 controls cardiac homeostasis and hypertrophy. *Circulation*. 2019;139:533–545. doi: 10.1161/CIRCULATIONAHA.118.036146
10. Li T, Zhuang Y, Yang W, Xie Y, Shang W, Su S, Dong X, Wu J, Jiang W, Zhou Y, et al. Silencing of METTL3 attenuates cardiac fibrosis induced by myocardial infarction via inhibiting the activation of cardiac fibroblasts. *FASEB J*. 2021;35:e21162. doi: 10.1096/fj.201903169R
11. Zhuang S, Ma Y, Zeng Y, Lu C, Yang F, Jiang N, Ge J, Ju H, Zhong C, Wang J, et al. METTL14 promotes doxorubicin-induced cardiomyocyte ferroptosis by regulating the KCNQ1OT1-miR-7-5p-TFRC axis. *Cell Biol Toxicol*. 2023;39:1015–1035. doi: 10.1007/s10565-021-09660-7
12. Min K-W, Zealy RW, Davila S, Fomin M, Cummings JC, Makowsky D, McDowell CH, Thigpen H, Hafner M, Kwon S-H, et al. Profiling of m^{6}A RNA modifications identified an age-associated regulation of AGO2 mRNA stability. *Aging Cell*. 2018;17:e12753. doi: 10.1111/acel.12753
13. Shafik AM, Zhang F, Guo Z, Dai Q, Pajdzik K, Li Y, Kang Y, Yao B, Wu H, He C, et al. N6-methyladenosine dynamics in neurodevelopment and aging, and its potential role in Alzheimer's disease. *Genome Biol*. 2021;22:17. doi: 10.1186/s13059-020-02249-z
14. Pan J-A, Tang Y, Yu J-Y, Zhang H, Zhang J-F, Wang C-Q, Gu J. miR-146a attenuates apoptosis and modulates autophagy by targeting TAF9b/P53 pathway in doxorubicin-induced cardiotoxicity. *Cell Death Dis*. 2019;10:668. doi: 10.1038/s41419-019-1901-x
15. Gupta SK, Garg A, Bär C, Chatterjee S, Foinquinos A, Milting H, Streckfuß-Bömeke K, Fiedler J, Thum T. Quaking inhibits doxorubicin-mediated cardiotoxicity through regulation of cardiac circular RNA expression. *Circ Res*. 2018;122:246–254. doi: 10.1161/circresaha.117.311335
16. Kusumoto D, Seki T, Sawada H, Kunitomi A, Katsuki T, Kimura M, Ito S, Komuro J, Hashimoto H, Fukuda K, et al. Anti-senescent drug screening by deep learning-based morphology senescence scoring. *Nat Commun*. 2021;12:257. doi: 10.1038/s41467-020-20213-0
17. Pfitzer L, Moser C, Gegenfurtner F, Arner A, Foerster F, Atzberger C, Zisis T, Kubisch-Dohmen R, Busse J, Smith R, et al. Targeting Actin inhibits repair of doxorubicin-induced DNA damage: a novel therapeutic approach for combination therapy. *Cell Death Dis*. 2019;10:302. doi: 10.1038/s41419-019-1546-9
18. Sedrak MS, Freedman RA, Cohen HJ, Muss HB, Jatoi A, Klepin HD, Wildes TM, Le-Rademacher JG, Kimmick GG, Tew WP, et al. Older adult participation in cancer clinical trials: a systematic review of barriers and interventions. *CA: Cancer J Clin*. 2021;71:78–92. doi: 10.3322/caac.21638
19. Henry ML, Niu J, Zhang N, Giordano SH, Chavez-MacGregor M. Cardiotoxicity and cardiac monitoring among chemotherapy-treated breast cancer patients. *JACC Cardiovasc Imaging*. 2018;11:1084–1093. doi: 10.1016/j.jcmg.2018.06.005
20. Feliu J, Heredia-Soto V, Gironés R, Jiménez-Munarriz B, Saldaña J, Guillén-Ponce C, Molina-Garrido MJ. Management of the toxicity of chemotherapy and targeted therapies in elderly cancer patients. *Clin Transl Oncol*. 2020;22:457–467. doi: 10.1007/s12094-019-02167-y
21. Zamorano JL, Lancellotti P, Rodriguez Muñoz D, Aboyans V, Asteggiano R, Galderisi M, Habib G, Lenihan DJ, Lip GYH, Lyon AR, et al. 2016 ESC position paper on cancer treatments and cardiovascular toxicity developed under the auspices of the ESC Committee for practice guidelines: the task force for cancer treatments and cardiovascular toxicity of the European Society of Cardiology (ESC). *Eur Heart J*. 2016;37:2768–2801. doi: 10.1093/eurheartj/ehw211
22. Gilchrist SC, Barac A, Ades PA, Alfano CM, Franklin BA, Jones LW, La Gerche A, Ligibel JA, Lopez G, Madan K, et al. Cardio-oncology rehabilitation to manage cardiovascular outcomes in cancer patients and survivors: a scientific statement from the American Heart Association. *Circulation*. 2019;139:e997–e1012. doi: 10.1161/CIR.0000000000000679
23. Ferreira de Souza T, Quinaglia AC, Silva T, Osorio Costa F, Shah R, Neilan TG, Velloso L, Nadruz W, Brenelli F, Sposito AC, et al. Anthracycline therapy is associated with cardiomyocyte atrophy and preclinical manifestations of heart disease. *JACC: Cardiovasc Imaging*. 2018;11:1045–1055. doi: 10.1016/j.jcmg.2018.05.012
24. Upadhyay S, Gupta KB, Mantha AK, Dhiman M. A short review: doxorubicin and its effect on cardiac proteins. *J Cell Biochem*. 2021;122:153–165. doi: 10.1002/jcb.29840
25. Zhu W, Shou W, Payne RM, Caldwell R, Field LJ. A mouse model for juvenile doxorubicin-induced cardiac dysfunction. *Pediatr Res*. 2008;64:488–494. doi: 10.1203/PDR.0b013e318184d732
26. Geula S, Moshitch-Moshkovitz S, Dominissini D, Mansour AA, Kol N, Salmon-Divon M, Hershkovitz V, Peer E, Mor N, Manor YS, et al. Stem cells. m^{6}A mRNA methylation facilitates resolution of naïve pluripotency toward differentiation. *Science*. 2015;347:1002–1006. doi: 10.1126/science.1261417
27. Lin S, Choe J, Du P, Triboulet R, Gregory RI. The m(6)a Methyltransferase METTL3 promotes translation in human cancer cells. *Mol Cell*. 2016;62:335–345. doi: 10.1016/j.molcel.2016.03.021
28. Chen X, Yu C, Guo M, Zheng X, Ali S, Huang H, Zhang L, Wang S, Huang Y, Qie S, et al. Down-regulation of m^{6}A mRNA methylation is involved in dopaminergic neuronal death. *ACS Chem Neurosci*. 2019;10:2355–2363. doi: 10.1021/acschemneuro.8b00657
29. Tang C, Xie Y, Yu T, Liu N, Wang Z, Woolsey RJ, Tang Y, Zhang X, Qin W, Zhang Y, et al. mA-dependent biogenesis of circular RNAs in male germ cells. *Cell Res*. 2020;30:211–228. doi: 10.1038/s41422-020-0279-8
30. Forrest RA, Swift LP, Rephaeli A, Nudelman A, Kimura K-I, Phillips DR, Cutts SM. Activation of DNA damage response pathways as a consequence of anthracycline-DNA adduct formation. *Biochem Pharmacol*. 2012;83:1602–1612. doi: 10.1016/j.bcp.2012.02.026
31. Koh J, Itahana Y, Mendenhall IH, Low D, Soh EXY, Guo AK, Chionh YT, Wang L-F, Itahana K. ABCB1 protects bat cells from DNA damage induced by genotoxic compounds. *Nat Commun*. 2019;10:2820. doi: 10.1038/s41467-019-10495-4
32. Moreno T, Monterde B, González-Silva L, Betancor-Fernández I, Revilla C, Agraz-Doblas A, Freire J, Isidro P, Quevedo L, Blanco R, et al. ARID2 deficiency promotes tumor progression and is associated with higher sensitivity to chemotherapy in lung cancer. *Oncogene*. 2021;40:2923–2935. doi: 10.1038/s41388-021-01748-y
33. Oba A, Shimada S, Akiyama Y, Nishikawaji T, Mogushi K, Ito H, Matsumura S, Aihara A, Mitsunori Y, Ban D, et al. ARID2 modulates DNA damage response in human hepatocellular carcinoma cells. *J Hepatol*. 2017;66:942–951. doi: 10.1016/j.jhep.2016.12.026
34. He L, Tian X, Zhang H, Hu T, Huang X, Zhang L, Wang Z, Zhou B. BAF200 is required for heart morphogenesis and coronary artery development. *PLoS One*. 2014;9:e109493. doi: 10.1371/journal.pone.0109493
35. Lin H, Zhu Y, Zheng C, Hu D, Ma S, Chen L, Wang Q, Chen Z, Xie J, Yan Y, et al. Antihypertrophic memory after regression of exercise-induced physiological myocardial hypertrophy is mediated by the long noncoding RNA Mhrt779. *Circulation*. 2021;143:2277–2292. doi: 10.1161/CIRCULATIONAHA.120.047000
36. Garry GA, Bezprozvannaya S, Chen K, Zhou H, Hashimoto H, Morales MG, Liu N, Bassel-Duby R, Olson EN. The histone reader PHF7 cooperates with the SWI/SNF complex at cardiac super enhancers to promote direct reprogramming. *Nat Cell Biol*. 2021;23:467–475. doi: 10.1038/s41556-021-00668-z
37. Gao R, Liang X, Cheedipudi S, Cordero J, Jiang X, Zhang Q, Caputo L, Günther S, Kuenne C, Ren Y, et al. Pioneering function of Isl1 in the epigenetic control of cardiomyocyte cell fate. *Cell Res*. 2019;29:486–501. doi: 10.1038/s41422-019-0168-1
38. Wu M, Peng S, Yang J, Tu Z, Cai X, Cai C-L, Wang Z, Zhao Y. Baf250a orchestrates an epigenetic pathway to repress the Nkx2.5-directed contractile cardiomyocyte program in the sinoatrial node. *Cell Res*. 2014;24:1201–1213. doi: 10.1038/cr.2014.113

39. Singh AP, Archer TK. Analysis of the SWI/SNF chromatin-remodeling complex during early heart development and BAF250a repression cardiac gene transcription during P19 cell differentiation. *Nucleic Acids Res*. 2014;42:2958–2975. doi: 10.1093/nar/gkt1232
40. Schick S, Rendeiro AF, Runggatscher K, Ringler A, Boidol B, Hinkel M, Májek P, Vulliard L, Penz T, Parapatics K, et al. Systematic characterization of BAF mutations provides insights into intracomplex synthetic lethalities in human cancers. *Nat Genet*. 2019;51:1399–1410. doi: 10.1038/s41588-019-0477-9
41. Lan Q, Liu PY, Haase J, Bell JL, Hüttelmaier S, Liu T. The critical role of RNA mA methylation in cancer. *Cancer Res*. 2019;79:1285–1292. doi: 10.1158/0008-5472.CAN-18-2965
42. Yue B, Cui R, Zheng R, Jin W, Song C, Bao T, Wang M, Yu F, Zhao E. Essential role of ALKBH5-mediated RNA demethylation modification in bile acid-induced gastric intestinal metaplasia. *Mol Ther Nucleic Acids*. 2021;26:458–472. doi: 10.1016/j.omtn.2021.08.019
43. Nie S, Zhang L, Liu J, Wan Y, Jiang Y, Yang J, Sun R, Ma X, Sun G, Meng H, et al. ALKBH5-HOXA10 loop-mediated JAK2 m^6A demethylation and cisplatin resistance in epithelial ovarian cancer. *J Exp Clin Cancer Res*. 2021;40:284. doi: 10.1186/s13046-021-02088-1
44. Meyer MR, Haas E, Barton M. Gender differences of cardiovascular disease. *Hypertension*. 2006;47:1019–1026. doi: 10.1161/01.HYP.0000223064.62762.0b
45. Su X, Shen Y, Jin Y, Kim I-m, Weintraub NL, Tang Y. Aging-associated differences in Epitranscriptomic m^6A regulation in response to acute cardiac ischemia/reperfusion injury in female mice. *Front Pharmacol*. 2021;12:654316. doi: 10.3389/fphar.2021.654316